*remote sensing*

MDPI

*Article*

# Consistency Analysis of the GNSS Antenna Phase Center Correction Models

**Renyu Zhou [1], Zhigang Hu [1], Qile Zhao [1,*], Hongliang Cai [2], Xuanzuo Liu [1], Chengyi Liu [1], Guangxing Wang [3], Haoyu Kan [1] and Liang Chen [4]**

[1] GNSS Research Center, Wuhan University, No. 129 Luoyu Road, Wuhan 430079, China; ry.zhou@whu.edu.cn (R.Z.); zhigang.hu@whu.edu.cn (Z.H.); liuxuanzuo@whu.edu.cn (X.L.); chengyiliu@whu.edu.cn (C.L.); kanhaoyu@whu.edu.cn (H.K.)
[2] Beijing Institute of Tracking&Telecommunication Technology, Beijing 100094, China; caibanyu@126.com
[3] School of Geography and Information Engineering, China University of Geosciences, Wuhan 430078, China; wanggx@cug.edu.cn
[4] School of Electronic and Information Engineering, Beihang University, 37 Xueyuan Road, Beijing 100191, China; sdkdchenliang@whu.edu.cn
* Correspondence: zhaoql@whu.edu.cn

**Abstract:** For the same antenna type, numerical differences among the phase center correction (*PCC*) models released by different institutes can reach several millimeters, which is far beyond the nominal calibration accuracy. This contribution introduces a new method to evaluate the consistency of these *PCC* models. We first investigated the coupling of phase center offset (*PCO*) and phase center variation (*PCV*) through simulation experiments, and the results show that the calibrated *PCO* values under different strategies may result in large differences, and so do *PCV* values due to strong coupling with *PCO*. This is further confirmed by field calibration experiments. Moreover, a new datum parameter is introduced to equivalently transform the *PCC* models to assess the consistency of *PCC* models of the same antenna type calibrated under different strategies or by different facilities. It is also essential to perform consistency analysis of *PCC* models in the coordinate domain. We further investigated these *PCC* models through a simulated positioning experiment. The results show that millimeter-level consistency of *PCC* models will lead to the same level of positioning precision in the coordinate domain. Moreover, as a comparison, both baseline positioning and PPP were performed with an antenna-type JAV_RINGANT_G3T NONE based on real observations. Multiday results showed that the average RMS of the positioning differences between *PCC* models from robot and anechoic chamber calibration is less than 1 mm for the baseline solution and 4 mm for the PPP solution, although the *PCC* model differences can reach 6 mm in L1 and 4 mm in L2, respectively. Finally, we also investigated the distribution of position biases without *PCC* or with inaccurate *PCC*. Considering the actual GPS constellation, we found that position biases have a strong correlation with latitude, if *PCV* values fluctuate greatly with the users' elevation angle.

**Keywords:** antenna phase center correction; phase center offset; phase center variation; consistency analysis; relative positioning; precise point positioning



**Citation:** Zhou, R.; Hu, Z.; Zhao, Q.; Cai, H.; Liu, X.; Liu, C.; Wang, G.; Kan, H.; Chen, L. Consistency Analysis of the GNSS Antenna Phase Center Correction Models. *Remote Sens.* **2022**, *14*, 540. https://doi.org/10.3390/rs14030540

Academic Editors: Raad A. Saleh, Xiaoxing He, Jean-Philippe Montillet, Zhao Li, Gaël Kermarrec, Rui Fernandes and Feng Zhou

Received: 21 November 2021
Accepted: 20 January 2022
Published: 23 January 2022



## 1. Introduction

With the development of the Global Navigation Satellite System (GNSS) and the emergence of more high-precision applications, more sophisticated models are required to address various errors, and the antenna phase center correction model is one of these vital models.

Phase center correction (*PCC*) aims to address the range error caused by the antenna phase center variation when transmitting and receiving GNSS signals. In the signal processing of an antenna, the real reception points of signals from different directions do not form an ideal hemisphere, which will cause delays or advances in phase observation. The

*PCC* magnitude can reach the decimeter level according to the antenna structure. Therefore, the *PCC* model must be carefully handled in applications where phase observations are involved.

In recent decades, various efforts have been devoted to calibrating *PCC* models. The initial antenna calibration is performed in an anechoic chamber [1–3] using simulated signals. Anechoic chamber calibration is viewed as a high-precision method. In the late 1990s, Mader [4] proposed a new kind of calibration method at the National Geodetic Survey (NGS) using a short baseline in the field. In this calibration, a specified Dorne Margolin choke ring antenna (AOAD/M_T) was assumed as the reference, and the *PCC* models to be estimated were all relative to this reference antenna. In addition, due to the static antenna and a similar satellite trajectory, this relative calibration cannot provide a full antenna phase center pattern with respect to both the elevation and azimuth angle. Wübbena et al. [5] and Menge et al. [6] proposed an absolute antenna calibration using an industrial robot. Benefiting from the swift motion of the robot, an absolute model is available and is free from the reference antenna.The absolute calibration model has been adopted by the International GNSS Service (IGS), and several institutions have provided absolute antenna calibration services.

In recent years, studies on the influences of the *PCC* model have drawn much attention. Bergstrand et al. [7] proposed a new method to evaluate the impact of the *PCC* model on the positioning. Krzan et al. [8] compared the differences between *PCC* models from field and chamber calibration for the same antenna. Darugna et al. [9] assessed the impact of absolute smartphone antenna calibration on high-precision positioning. Villiger et al. [10] studied GNSS scale determination with antenna patterns for the Galileo system.

## 2. Phase Center Correction Model

### *2.1. Phase Center Model*

The *PCC* model [11] widely adopted by the GNSS community is shown in Figure 1. In the spatial hemisphere above the antenna, an accessible point is defined as the antenna reference point (ARP), and a three-dimensional vector from the ARP to the average phase receiving center is defined as the phase center offset (*PCO*), and the range variation in the phase observation in different directions based on *PCO* is defined as the phase center variation (*PCV*). *PCC* is described in the antenna body system. The $x$-axis of the frame points from ARP to the north reference marker (NRP) of the antenna while the $z$-axis points from ARP to the boresight of the antenna. The $y$-axis together with the $x$-axis and $z$-axis form a left-hand coordinate system. If the antenna is placed at a station and oriented correctly, the antenna system is aligned to the local north-east-up system of the station. According to this *PCC* model, users can correct the phase observation while considering the relative attitude between the satellite and ground antenna. With the help of *PCC* models, GNSS-based applications with different antennas can reach a clear and consistent solution, which can reduce systematic bias and improve the positioning accuracy.

Considering that the wavefront of all signals can form a series of concentric circles, range deviations from two arbitrary wavefronts with certain distances are equivalent in any direction. It is necessary to consider this kind of constant range bias to construct a comprehensive understanding of the *PCC* model. Therefore, in addition to the traditional *PCO*/*PCV* sets, another datum parameter, denoted as B, is introduced in this contribution to help the analysis and evaluation of the *PCC* model. It should be emphasized that this datum B in the *PCC* model will not affect the position estimates. In single point positioning, B will be perfectly absorbed into the receiver clock or ambiguity while in relative positioning, B will be eliminated if differencing between satellites is performed. In this contribution, B is used as a tool to aid in evaluating and analyzing the *PCC* model.

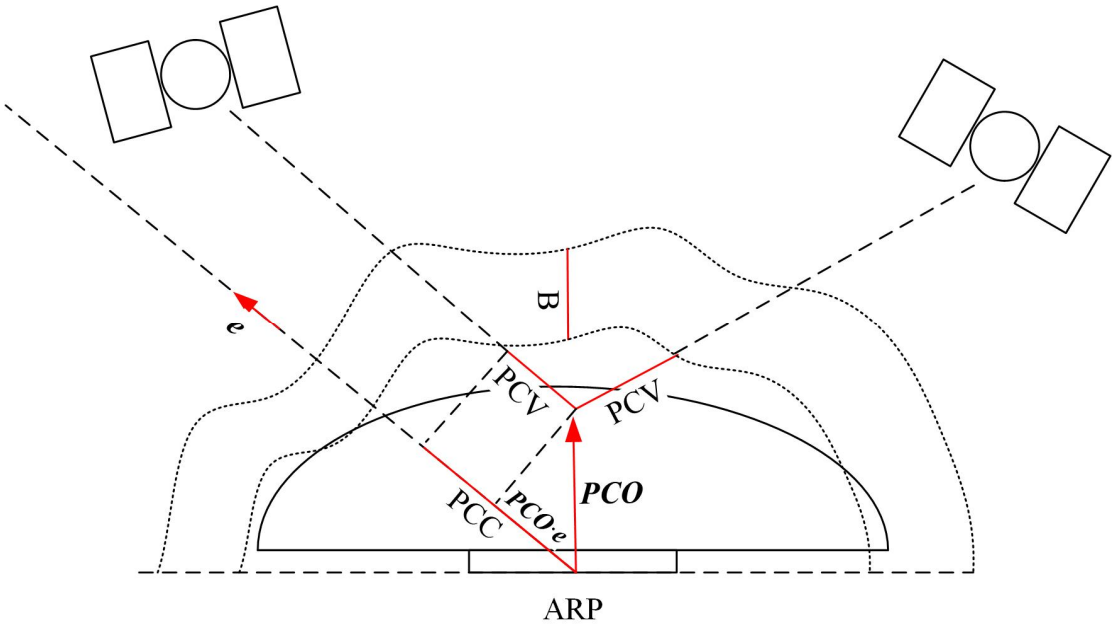


**Figure 1.** Antenna phase center correction model. *PCO* is a vector pointing from antenna reference point (ARP) to mean phase center while *PCV* is the range variation based on *PCO*; B denotes the datum; $e$ denotes the directional vector from antenna to satellite.

The computation of *PCC* can be expressed as:

$$PCC(\alpha, z) = -PCO \cdot e + PCV(\alpha, z) + B \tag{1}$$

where *PCO* is a three-dimensional vector in local north-east-up coordinates, and *PCV* is a range correction, usually in a tabular format. Thus, *PCV* needs to be interpolated through values at surrounding grid points; $B$ is the unknown datum constant; $e$ denotes the directional vector from the ground antenna to the satellite. $\alpha$ and $z$ denote the azimuth and zenith angles, respectively, and $e$ can be expressed by $\alpha$ and $z$ as:

$$e = \{\sin(z)\cdot\cos(\alpha), \sin(z)\cdot\sin(\alpha), \cos(z)\} \tag{2}$$

In the typical *PCC* model concept, it is assumed that no deviation exists in the zenith direction, which means that $B$ is zero. When using the *PCC* model, this practice will not affect the position estimates while in antenna calibration, a zero *PCV* constraint in the zenith direction is one of the necessary demands for the *PCV* estimation to set a *PCV* datum and avoid rank defects of the normal equation. In other words, a constraint of $B$ as 0 in the zenith direction is reasonable and feasible in practice, although $B$ might not be zero. It will make sense when transforming the *PCC* model from a set of *PCO*/*PCV* to another set while keeping the consistency between them, and their coupling features will be investigated in the following sections.

### *2.2. Differences in Different IGS ANTEX Versions*

At present, several institutions have accomplished antenna field calibration and released *PCC* models in research or commercial methods, including Geo++ [12], NGS [13], Institut für Erdmessung, Leibniz University Hannover (IfE) [14], Geoscience Australia [15], and Senatsverwaltung für Stadtentwicklung und Wohnen (SenStadt), Berlin. However, differences do exist between *PCC* models from different institutions and calibration methods [7]. As the largest GNSS research community, the IGS also adopts more than 300 *PCC* models from those institutions and releases them to promote GNSS research. Since 2005, igs05.atx, igs08.atx, and igs14.atx have been successively released by the IGS, which are in accordance with the corresponding International Terrestrial Reference Frame (ITRF).

In 2019, IGS released igsR3.atx as a part of the ReProcess3 Campaign that comprises the newest *PCC* models of multi-GNSS and multifrequency [10]

Investigating the *PCC* models released by IGS, differences in *PCO*s with a magnitude exceeding 1 mm can be found for some receiver antennas between different versions of the antenna file in the antenna exchange format (ANTEX) [16]. Taking igs14.atx as a reference, *PCO* differences in the robot calibration models from igs05.atx, igs08.atx, and igsR3.atx have been calculated and are shown in Figure 2. For more than 40 *PCC* models, the magnitudes of the *PCO* shifts among different versions exceeds 1 mm. In general, the shifts in the north and east components are less than or approximately 1 mm except for antenna JAV_GRANT-G3T NONE. The *PCO* shifts in the up component can reach 4 mm, which are comparably larger. In addition, it can be seen in Figure 2 that the magnitude of the *PCO* shift with an L2 frequency is larger than that with L1, which may imply that a higher precision and stability of the *PCC* model in L1 can be expected compared with L2. The *PCO* estimates are quite stable, and the repeatability of calibration is better than 1 mm or even 0.5 mm. This contradiction may cause some confusion and undermine the user's confidence in the consistency of *PCC* models.

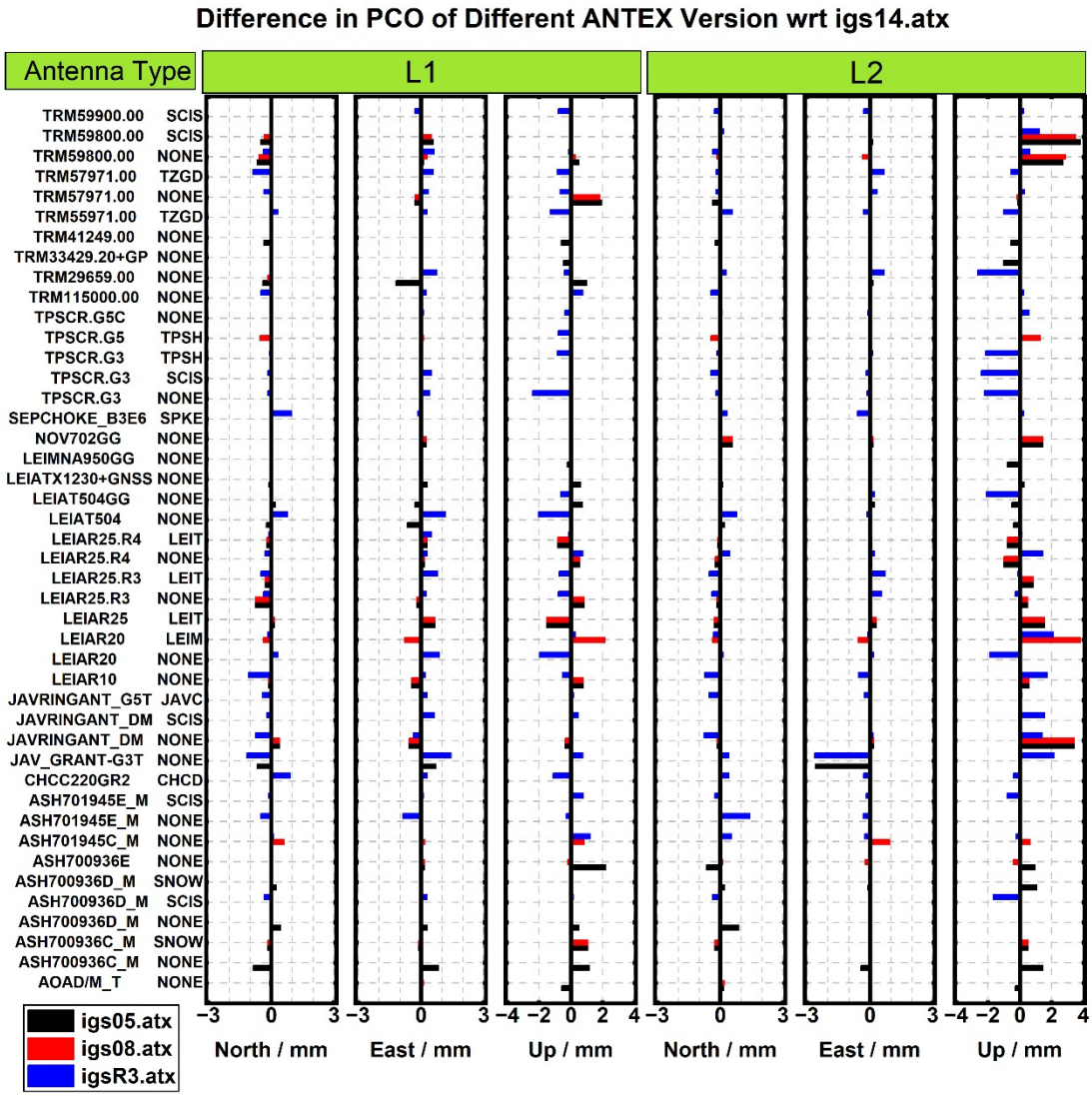


**Figure 2.** Differences in *PCO* for different *PCC* models in different ANTEX versions.

In the comparison, an extreme example of a *PCC* model for the antenna type JAV_RINGANT_G3T NONE is found between robot calibration from igs14.atx and ane-

choic chamber calibration from igsR3.atx. As listed in Table 1, the numerical differences in *PCO* in L1 and L2 apparently exceed 1 mm. Taking the differences in L1 as an example, differences in the north, east, and up components reach (−0.21, 0.05, −6.02) mm, respectively. The convention of $PCV(\alpha, z)|_{z=0} = 0$ is not followed by the anechoic chamber calibration, and datum of 3 mm can be found. Therefore, these two models are quite different and a low consistency between them is seen in the elevation-dependent *PCV* shown in Figure 3. We will investigate the consistency of this example in detail in the following section.

**Table 1.** Differences between igs14.atx and igsR3.atx of *PCO* and datum B for Antenna JAV_RINGANT_G3T NONE (unit:mm).

| *PCC* | L1 | | | | L2 | | | |
|---|---|---|---|---|---|---|---|---|
| | **N** | **E** | **U** | **B** ($PCV_{z=0}$) | **N** | **E** | **U** | **B** ($PCV_{z=0}$) |
| igs14.atx | 0.25 | 2.24 | 49.04 | 0 | 6.80 | −3.16 | 54.72 | 0 |
| igsR3.atx | 0.46 | 2.19 | 55.06 | 3 | 6.25 | −2.97 | 58.58 | 2.46 |
| Difference | −0.21 | 0.05 | −6.02 | −3 | 0.55 | −0.19 | −3.86 | −2.46 |

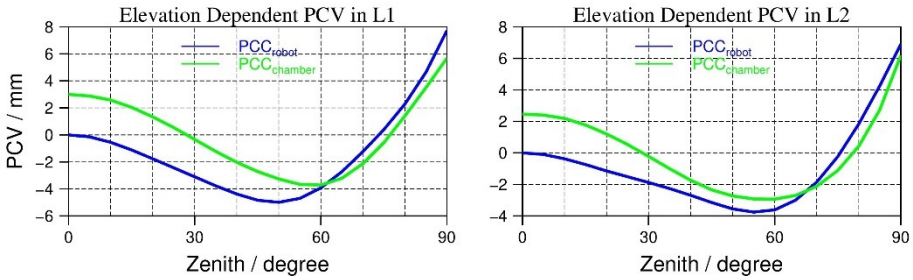


**Figure 3.** Difference in the elevation-dependent *PCV* for JAV_RINGANT_G3T NONE between robot calibration (from igs14.atx) and anechoic chamber calibration (from igsR3.atx).

Considering the variations and discrepancies shown in the previous context, it may cause problems for users when choosing an appropriate *PCC* model. This contribution focuses on the analysis and investigation of the correlation of *PCO*/*PCV* sets and aims to find a proper method to evaluate *PCC* models, including the consistency and impact on positioning.

## 3. Methodologies and Experiment Design

Motivated by the relatively large difference between different *PCC* models for the same antenna, we designed the simulation experiment described in the following subsection to investigate the possible reason for this difference and how to evaluate the consistency between these models.

The analysis and evaluation of the *PCC* model are mainly based on two simulation experiments of *PCC* estimation and point positioning. In the simulation of *PCC* estimation, virtual *dPCC* observations are constructed from the original *PCC* model released by IGS, and then new *PCC* models are estimated with different strategies. In the simulated positioning experiment, virtual ranging observations are constructed from two *PCC* models, and point positioning is performed to evaluate the differences in the two *PCC* models in the coordinate domain. In this section, we mainly introduce our methodologies and the design of the simulation experiment for *PCC* estimation and positioning as shown in Figure 4, and the details will be described in the following sections.

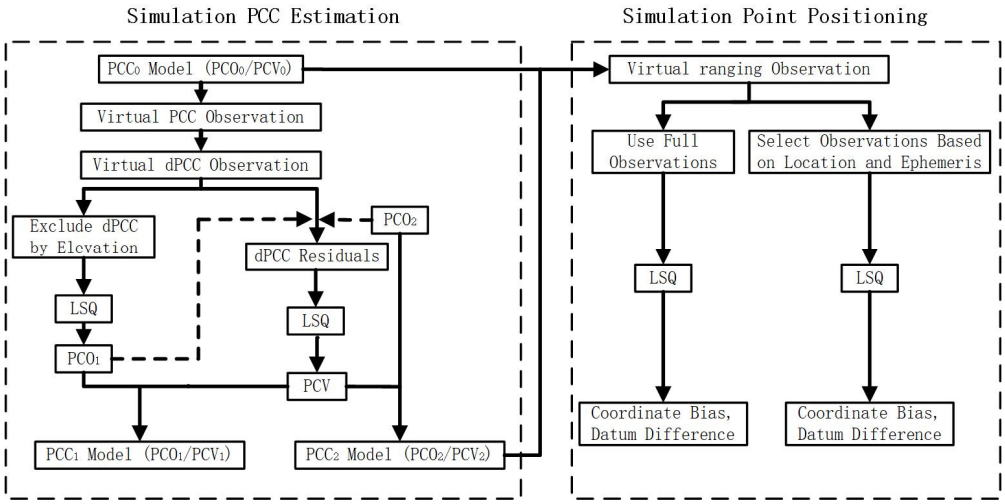


**Figure 4.** Design of the simulation experiment for *PCC* estimation and point positioning.

### *3.1. Simulation of PCC Model Estimation*

Based on the existing *PCC* model from the IGS, a special experiment using virtual observation is designed to simulate the *PCC* calibration and investigate the factors that might be responsible for different calibrations.

The specially simulated calibration follows two steps. First, we compute virtual *PCC* and *dPCC* observations according to Equation (1) from the existing *PCC* models as will be described in Section 3.1.1. Second, estimation of *PCO*/*PCV* is implemented under different strategies, and the estimation process is presented in Section 3.1.2.

#### 3.1.1. Virtual Differenced *PCC* Observation

In the simulation, a virtual antenna with the model $PCC_0(PCO_0/PCV_0)$ is placed in a north-east-up coordinate system to observe a virtual satellite $i$ with direction $(z^i, \alpha^i)$, where $z^i$ and $\alpha^i$ are the zenith and azimuth angles, respectively. The corresponding virtual ranging observation $PCC_0$ $(z^i, \alpha^i)$ calculated according to Equation (1) is called the virtual *PCC* observation. Since the datum $B$ is arbitrary and cannot be determined, differencing between different satellites is performed, which is commonly applied in real field calibration [17,18]. Another virtual satellite $j$ at direction $(z^j, \alpha^j)$ is introduced as a reference. To estimate the *PCO*/*PCV* set, the virtual differenced *dPCC* observation is required and can be obtained as:

$$\begin{aligned} dPCC(\alpha^i, z^i) &= PCC_0(\alpha^i, z^i) - PCC_0(\alpha^j, z^j) \\ &= -PCO_0 \cdot (e^i - e^j) + [PCV_0(\alpha^i, z^i) - PCV_0(\alpha^j, z^j)] \end{aligned} \quad (3)$$

where $e$ is the line-of-sight vector from the virtual antenna to the virtual satellite. The benefit of using a virtual observation is to avoid irrelevant errors, such as atmospheric delay, clock, multipath, and observation noise, and only the mutual influence imposed by *PCO*/*PCV* and their relation are revealed through this experiment.

If the directions of satellite $i$ and $j$ are too close, the elements of $(e^i - e^j)$ will be close to 0 and introduce disturbance in the estimation process. To avoid the two signal directions getting too close, two arbitrary reference directions are selected. The first reference satellite is located at (30°, 45°) in zenith and azimuth while the second is (60°, 225°). Virtual observations with zenith angles larger than 45° are differenced with the first reference satellite while those with zenith angles smaller than 45° are differenced with the second reference satellite. Thus, all *dPCC*s are constructed in this way.

#### 3.1.2. *PCO* and *PCV* Estimation

From the virtual *dPCC* observation in Equation (3), the *PCO* and *PCV* parameters are estimated. Since *PCO* and *PCV* are both related to the satellite direction, they are highly

coupled. Therefore, the estimation is divided into two steps following similar procedures to real field calibration [13,18] to investigate the consistency of different *PCO*/*PCV* and its correlation.

When the *PCO* is estimated, the *PCV* part is omitted. The vector to be estimated is defined as $PCO_1$ = (n, e, u), and the three components are the projections of $PCO_1$ onto the north, east, and up directions, respectively. The coefficient $H_i$ of $PCO_1$ for the $dPCC^{\mathrm{i}}$ is expressed as:

$$\begin{aligned} H_i = e^i - e^j \quad &= \left\{sin\left(z^i\right) \cdot cos\left(\alpha^i\right), sin\left(z^i\right) \cdot sin\left(\alpha^i\right), cos\left(z^i\right)\right\} \\ &-\left\{sin\left(z^j\right) \cdot cos\left(\alpha^j\right), sin\left(z^j\right) \cdot sin\left(\alpha^j\right), cos\left(z^j\right)\right\} \end{aligned} \tag{4}$$

The spatial hemisphere above the antenna is divided into grids of 5° in zenith by 5° in azimuth, and for each satellite $i$ ($i$ = 1, 2, . . . , $n$), the virtual ranging observation $dPCC^{\mathrm{i}}$ is calculated at the corresponding grid. Thus, the design matrix $H$ and error vector $V$ are defined as:

$$\begin{cases} H = \left\{H_0^T, \ldots, H_n^T\right\}^T \\ V = \left\{dPCC_0, \ldots, dPCC_n\right\}^T \end{cases} \tag{5}$$

Moreover, from Equation (5), $PCO_1$ is obtained with a least-square adjustment (LSQ) as:

$$PCO_1 = \left(H^T \times H\right)^{-1} \times \left(H^T \times V\right) \tag{6}$$

For the *PCV* estimation, the *PCO* part in the *dPCC* observation should be corrected. We substitute the $PCO_1$ estimated from Equation (6) into Equation (3), and the residuals of *dPCC* from which the *PCV* will be extracted are computed as:

$$\begin{aligned} Res_i \quad &= dPCC\left(\alpha^i, z^i\right) + PCO_1 \cdot \left(e^i - e^j\right) \\ &= \left[PCV_0\left(\alpha^i, z^i\right) - PCV_0\left(\alpha^j, z^j\right)\right] - \left(PCO_0 - PCO_1\right) \cdot \left(e^i - e^j\right) \end{aligned} \tag{7}$$

Considering that *PCV* is a ranging deviation of different directions above the antenna, it is a function of azimuth $\alpha$ and zenith $z$, which can be appropriately expressed with a set of spherical harmonics (SH) in this estimation. The general form of *PCV* is expressed as:

$$PCV(\alpha, z) = \sum_{n=0}^{nmax} \sum_{m=0}^{n} \left(C_{n,m} \cdot cosm\alpha + S_{n,m} \cdot sinm\alpha\right) \cdot P_{n,m}(cosz) \tag{8}$$

where $C_{n,m}$ and $S_{n,m}$ are the corresponding spherical harmonics that need to be estimated, $n$ and $m$ are the order and degree of the spherical harmonics that meet the condition of $m \leq n$, and $P_{n,m}$ is the Legendre polynomials. Similar to the practice of real *PCC* calibration, spherical harmonics of order 8 and degree 8 are used in this experiment.

To avoid rank deficiency of the normal equation, a special tight constraint of zero *PCV* in the zenith direction is applied as:

$$PCV(0, \alpha) = \textstyle\sum_{n=0}^{nmax} C_{n,0} \cdot P_{n,0}(1) = 0 \tag{9}$$

With a similar LSQ process for *PCO* estimation, the coefficients $C_{n,m}$ and $S_{n,m}$ can be obtained, and then the *PCV* at any direction can be calculated according to the spherical harmonics. Thus, $PCV_1$ is obtained together with $PCO_1$, and a new antenna model $PCC_1(PCO_\mathbf{1}/PCV_1)$ is therefore estimated from the *dPCC* observation constructed by $PCC_0(PCO_0/PCV_0)$.

It should be noted that if any other set of $PCO_2$ is introduced in Equation (7), a corresponding $PCV_2$ will be obtained and lead to the antenna model $PCC_2(PCO_2/PCV_2)$. Therefore, we will intentionally adjust the $PCO_2$ in the estimation of *PCV*, and investigate the correlation between the variation in *PCO* and *PCV*.

### *3.2. Simulation of Point Positioning*

As described in Section 3.1, the antenna model *PCC* obtained from the simulation estimation is obviously different in numerical values in terms of *PCO* or *PCV* compared with the original model if a different *PCO* is introduced in the *PCV* estimation. We want to investigate the consistency of these different *PCC* models on positioning. Therefore, a simulated point positioning is designed.

Given two antenna models $PCC_0$ and $PCC_1$ with certain differences in *PCO* and *PCV*, we assume an antenna with $PCC_1$ is placed in the north-east-up coordinate system to track the signal from a virtual satellite $i$ with zenith $z^i$ and azimuth $\alpha^i$, and the virtual ranging observation is $PCC_0$; thus, the equation of the virtual ranging observation $V^i$ is written as:

$$V^i = PCC_0^i(\alpha,\ z) - PCC_1^i(\alpha,\ z) = -e \cdot [dn, de, du] - \nabla B \tag{10}$$

Here, the parameters to be estimated are denoted as $X = (dn, de, du, \nabla B)$, specifically the coordinate biases $(dn, de, du)$ along with the datum difference $\nabla B$. The coefficient $H_i$ of $X$ for $V^i$ is written as:

$$H_i = [-e, -1] = [-sin(z) \cdot cos(\alpha), -sin(z) \cdot sin(\alpha), -cos(z), -1] \tag{11}$$

If more than four satellites are observed, $X$ can be estimated. Therefore, more virtual satellites are distributed at different directions in the upper hemisphere. The design matrix $H$ and error vector $V$ for all virtual ranging observations of satellites in the point position experiment are obtained as:

$$\begin{cases} H = \left[H_1^T, \ldots, H_n^T\right]^T \\ V = \left[V_1, \ldots, V_n\right]^T \end{cases} \tag{12}$$

Finally, the coordinate biases are obtained through a least-square adjustment process as:

$$X = \left(H^T \times H\right)^{-1} \times \left(H^T \times V\right) \tag{13}$$

Coordinates biases estimated in this virtual point positioning simulation can be viewed as an indicator of the differences in $PCC_0$ and $PCC_1$ in the coordinate domain.

## 4. Coupling Analysis of *PCO* and *PCV* Parameters

To validate and compare the mutual influence between *PCO* and *PCV* in the calibration, several types of experiments are designed and implemented as described in Section 3. The original *PCC* models are based on igs05.atx, igs08.atx, igs14.atx, and igsR3.atx released by IGS (https://files.igs.org/pub/station/general/, accessed on 18 January 2022). In addition, absolute antenna calibration was implemented at Wuhan University [18], and multi-GNSS *PCC* model calibration is currently under testing. Benefiting from previous work, the impact of *PCO* and *PCV* on calibration can be investigated through field GNSS data. Particularly, in this contribution, the field calibration data for TRM59800.00 NONE were collected on DoY (Day of Year) 332 in 2020, and the timespan was 24 h.

### *4.1. PCO Estimation by Different Elevation Masks*

The estimates of $PCO_1$ will be precisely equal to $PCO_0$ if *dPCC* observations are constructed from $PCC(PCO_0/PCV_0)$, where $PCV_0$ are all zero. However, the *PCV* parts are non-zero and will cause differences in the *PCO* estimates. In the real data processing of field calibration, as different elevation masks are applied, the *dPCC* observations containing different *PCV*s are changed in the *PCO* estimation. Therefore, *PCO* estimates might vary as different elevation masks are applied. In this virtual simulation experiment, we set an elevation mask to control the computation of the virtual *dPCC* observation and investigate the differences in the *PCO* estimates as a function of the elevation mask.

Following the steps described in Section 3.1, the *PCO* estimates of antenna TRM59800.00 NONE from the virtual *dPCC* observation are analyzed as a detailed example shown in

the left panel of Figure 5 while the right panel shows the real calibration in the field. The trends for the simulated estimation and field calibration are similar. As the elevation mask angle increases, biases change slowly in the north and east components but decrease sharply in the up component. The field calibration curve is smoother than that of the simulated estimation. *PCO* estimation in the up component is apparently more vulnerable and sensitive to the elevation cutoff angle than the other two components. In the simulation estimation, since there is no other error or noise in the virtual *dPCC* observation, the biases must be caused by the only disturbance of *PCV* that is ignored in the process. In both the simulation estimation and field calibration, the *PCO* biases with L1 varies more significantly than those with L2, which coincides with the fact that the absolute *PCV* value for L1 is larger than that for L2. It can be concluded that the variation in *PCO* biases is highly dependent on the *PCV* magnitude.

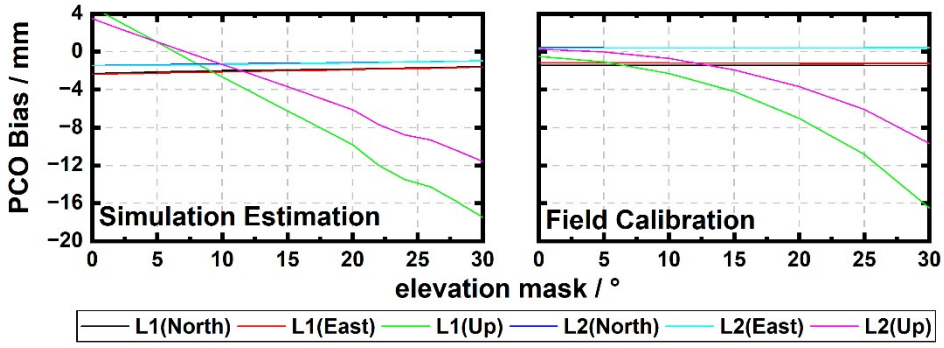


**Figure 5.** Difference between *PCO* estimates and the original value in igs14.atx for L1/L2 as a function of different elevation masks.

Furthermore, we performed the *PCO* estimation for all *PCC* models presented in igs14.atx and set the elevation mask as zero degrees. Differences exceeding 1 mm in the up component of *PCO* estimates of approximately 140 antennas are shown in Figure 6. Except for several types, the estimates of the up components for most of the antennas are larger than their original values and can reach 3~6 mm. However, the precision of field *PCO* estimation can reach the 1 mm level or even better than 0.5 mm. In this simulation estimation, the *PCO* estimates might not be equal to the values used to construct the virtual *dPCC* observation, although only the *PCC* without any external error is induced in the simulation. It suggests that the *PCC* calibration might lead to different *PCO* estimates due to different process strategies, which indicate a low stability for different calibration strategies. The neglecting or partial selection of *dPCC* observations can cause a significant disturbance in the *PCO* estimates.

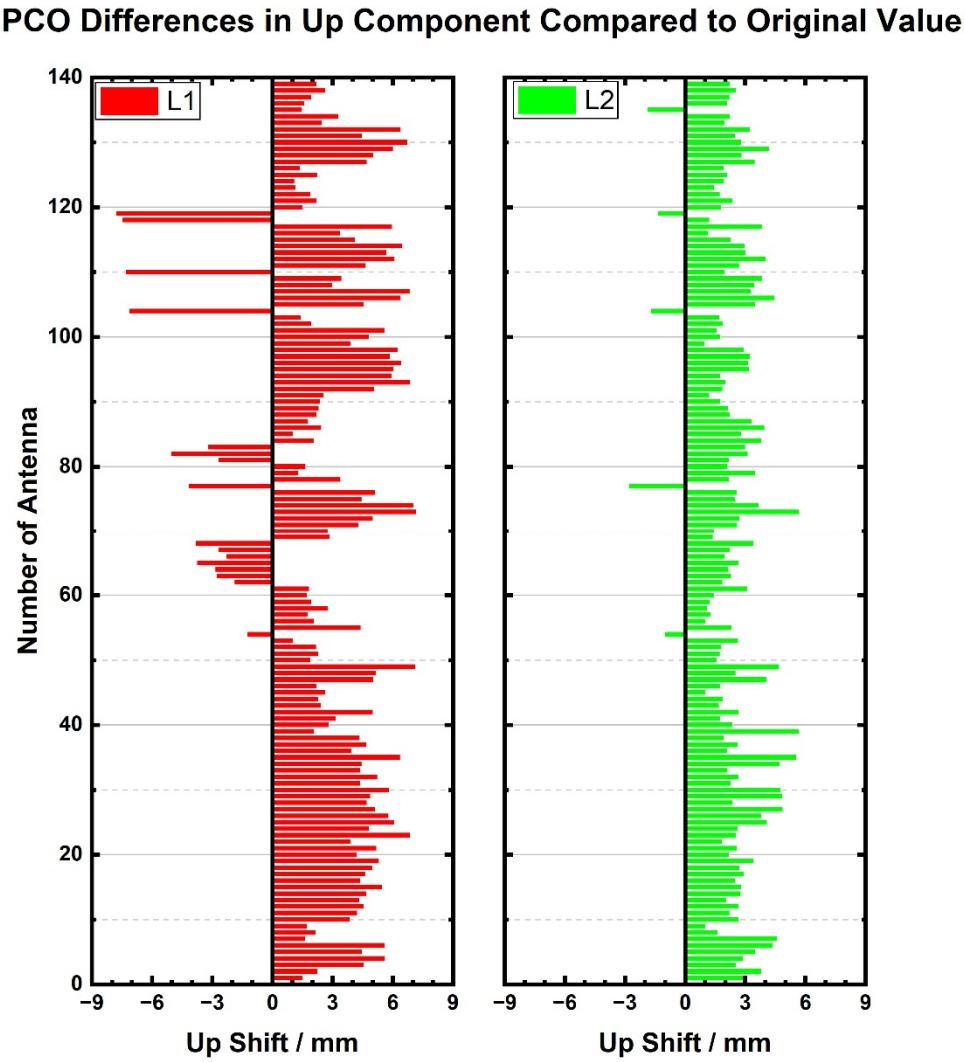


**Figure 6.** Differences in the up component of *PCO* estimates compared with its original value for antennas in igs14.atx.

### *4.2. Coupling of PCO Shifts and PCV Variation*

According to the discussion in the previous section, the estimated *PCO* will be affected while *PCV* is ignored in the *dPCC* observation. Since the estimated *PCO* is introduced into the *dPCC* observation to compute residuals for the estimation of *PCV*, different *PCO*s might lead to different *PCV* estimations. The relation between variations in *PCO* and *PCV* will be analyzed.

Since the *PCO* is dominant in the up component, several intentional shifts were added to the up component of the original *PCO* value in this experiment and introduced back into the estimation of *PCV*. Comparison was made between the *PCV* estimates afterward. Following the steps described in Section 3.1, we performed the *PCV* estimation of antenna TRM59800.00 and the original model $PCC_0$ in igs14.atx is used in this experiment. Specifically, shifts from −10 to 10 mm with an interval of 1 mm are added to the up component of $PCO_0$ to obtain $PCO_s$, and $PCO_s$ is then introduced into the computation of *dPCC* residuals. The elevation-dependent *PCV* estimation is shown in the left column of Figure 7 while the *PCV* estimation from field calibration is placed in the right column.

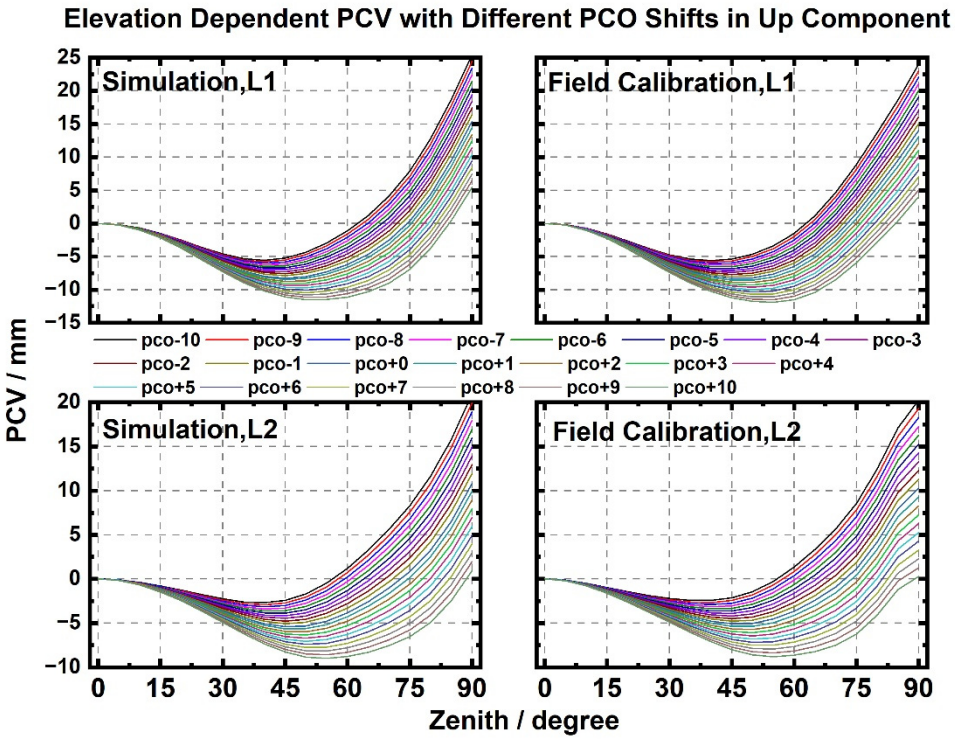


**Figure 7.** *PCV* curve variation with different *PCO* bias in the up component.

The elevation-dependent *PCV* curves are nearly the same for the simulation estimation and field calibration. It can be clearly seen that the variations in the elevation-dependent *PCV* curves with different *PCO* shifts *s* are similar. All curves start from zero in the zenith direction due to the tight constraint of zero *PCV* in the zenith direction. As the zenith increases, the curves diverge from each other, and the width of the spacing expands. At a certain zenith, the *PCV* value increases as the intentional shift decreases, and all *PCV* values are evenly spaced. When the zenith angle reaches 90 degrees, the distances between adjacent curves are all 1 mm, which is precisely the interval of the intentional shifts. From the apparent negative correlation between the *PCO* shift and *PCV* value, it can be safely assumed that the *PCO* shifts can be perfectly compensated by the *PCV* estimates. In this sense, only if the *dPCC* observation is correct or consistent can the separation of *PCC* lead to several equivalent $PCO/PCV$ sets even with a large numerical difference in individual *PCO* or *PCV* values.

In fact, the relation between the *PCO* shift and the *PCV* value can be deduced theoretically according to [19], and the transformation from one $PCC_1(PCO_1/PCV_1)$ to another $PCC_2(PCO_2/PCV_2)$ with $d_{pco} = PCO_2 - PCO_1 = (d_N, d_E, d_U)$ is based on Equation (1) as:

$$\begin{aligned} PCC(\alpha, z) &= -PCO_1 \cdot e + PCV_1(\alpha, z) + B_1 \\ &= -\left(PCO_2 - d_{pco}\right) \cdot e + PCV_1(\alpha, z) + B_1 \\ &= -PCO_2 \cdot e + \left[PCV_1(\alpha, z) + d_{pco} \cdot e + d_B\right] + (B_1 - d_B) \\ &= -PCO_2 \cdot e + PCV_2(\alpha, z) + B_2 \end{aligned} \tag{14}$$

Therefore,

$$\begin{cases} PCV_2(\alpha, z) = PCV_1(\alpha, z) + d_{pco} \cdot e + d_B \\ B_2 = B_1 - d_B \end{cases} \tag{15}$$

To conform with the convention of $PCV_1(\alpha, 0) = PCV_2(\alpha, 0) = 0$,

$$\begin{aligned} PCV_2(\alpha, 0) &= PCV_1(\alpha, 0) + d_{pco} \cdot e + d_B \\ &= 0 + (d_N, d_E, d_U) \cdot (e_N, e_E, e_U) + d_B \\ &= (d_N, d_E, d_U) \cdot (\sin 0 \cos \alpha, \sin 0 \sin \alpha, \cos 0) + d_B \\ &= d_U + d_B = 0 \end{aligned} \tag{16}$$

This condition leads to:

$$d_B = -d_U \tag{17}$$

and,

$$PCV_2(\alpha, z) = PCV_1(\alpha, z) + d_{pco} \cdot e - d_U \tag{18}$$

Particularly, if a shift $d_U$ is added to the upper component of $PCO$, i.e., $d_{pco} = (0, 0, d_U)$, a simplified relation between $PCV_1$ and $PCV_2$ is obtained as:

$$PCV_2(\alpha, z) = PCV_1(\alpha, z) - d_U \cdot (1 - \cos(z)) \tag{19}$$

Regarding the shift $d_N$ or $d_E$, they will not influence the average $PCV$ at a certain zenith since:

$$\begin{cases} \int_0^{2\pi} (d_N \cdot \mathrm{sinzcos}\alpha) d\alpha = 0 \\ \int_0^{2\pi} (d_E \cdot \mathrm{sinzsin}\alpha) d\alpha = 0 \end{cases} \tag{20}$$

However, it will obviously affect the $PCV$ value at the same zenith, and whether it is amplified or reduced will depend on $d_N$, $d_E$ and the original $PCV$ value.

Considering the extreme example JAV_RINGANT_G3T NONE mentioned in Section 2.2, this transformation is applied and the differences will be investigated. The anechoic chamber calibration from igsR3.atx is denoted as $PCC_1(PCO_1/PCV_1)$ while robot calibration from igs14.atx is denoted as $PCC_2(PCO_2/PCV_2)$. To align $PCC_1$ to $PCC_2$ with the same $PCO_2$, several operations were performed and L1 was taken as an example. First, the difference in datum B of 3 mm is subtracted from all the $PCV$ of $PCC_1$ to obtain $PCC_3(PCO_\mathbf{1}/PCV_3)$. $PCV_3$ follows the convention of zero $PCV$ at a zero zenith angle, and is equivalent to $PCC_1$ in terms of positioning. The 3 mm datum differences can be absorbed into the clock or ambiguity. Second, we add $d_{pco}$ to $PCO_1$ and correct the $PCV_3$ value at each grid point according to Equation (18) to obtain $PCC_4(PCO_2/PCV_4)$ while $d_{pco}$ is the differences between $PCO_\mathbf{1}$ and $PCO_\mathbf{2}$. Here, in this case, $d_{pco}$ for L1 is (−0.21 mm, 0.05 mm, −6.02 mm) as listed in Table 1. Finally, the same $PCO_2$ is set for robot calibration $PCC_2(PCO_2/PCV_2)$ and transformed anechoic chamber calibration $PCC_4(PCO_2/PCV_4)$. $PCV_2$ and $PCV_4$ can be directly differenced and compared with common $PCO_2$. The procedures of this alignment are shown in Figure 8, and the differences in robot calibration and anechoic chamber calibration before and after the alignment for JAV_RINGANT_G3T NONE are presented in Figure 9.

As can be seen in Figure 9, obvious numerical differences exceeding 3 mm in $PCV$ between $PCC_1$ and $PCC_2$ can be found for both L1 and L2. After the operations described before, $PCC_1$ is aligned to $PCC_2$ with the same $PCO_2$, and differences in $PCV$ are dramatically decreased to approximately 1 mm except for some areas with low elevation. This case can be an example to validate the equivalence of $PCC$ models with large numerical differences in $PCO/PCV$ and the correctness of the alignment methods. Therefore, $PCC$ models with large numerical differences can still be approximately equivalent models if the alignment procedures decrease the differences to a 1 mm level. This practice can provide an approach to compare the $PCV$ with $PCO$ aligned rather than comparing $PCO$ and $PCV$ separately, and it can avoid false judgment caused by a direct discrepancy in $PCO$ or $PCV$, and reveal the overall differences with consideration of both $PCO$ and $PCV$ combined.

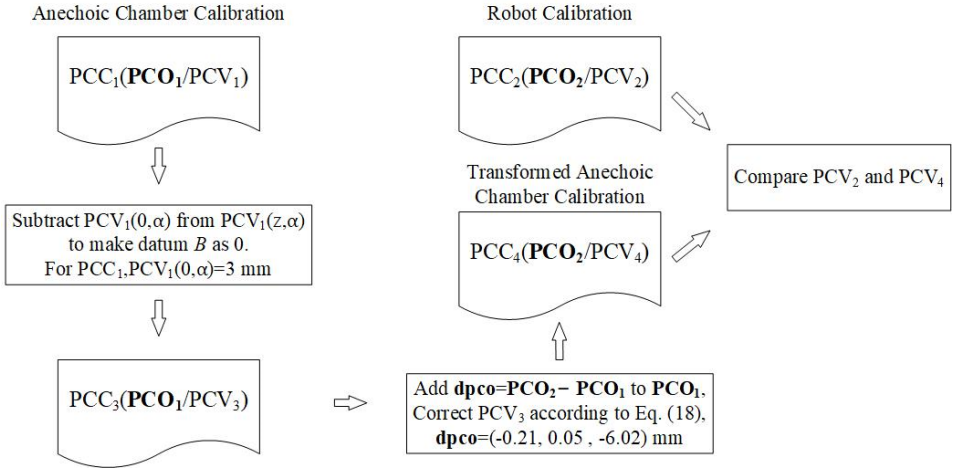


**Figure 8.** Procedures of aligning the *PCC* model of anechoic chamber and robot calibration with the same *PCO* for antenna JAV_RINGANT_G3T NONE.

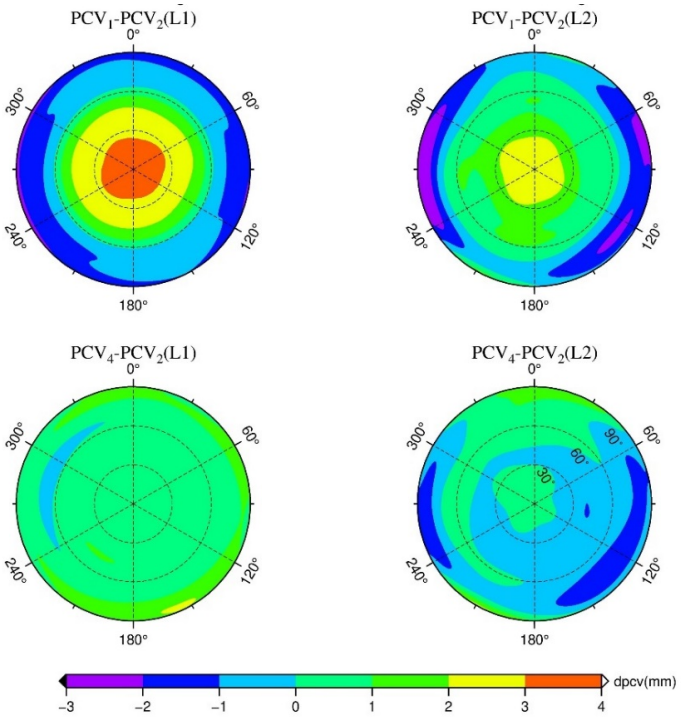


**Figure 9.** Differences in the *PCC* model between robot and chamber calibration for antenna JAV_RINGANT_G3T NONE before and after alignment. $PCV_1$ and $PCV_4$ are from the anechoic chamber calibration before and after *PCO* aligned to the same as robot calibration, $PCV_2$ is from the robot calibration.

## 5. Impact of Equivalent *PCC* Models on Positioning

Although biases of magnitude up to the millimeter or even centimeter level may exist in *PCC* models from different institutions due to different calibration conditions and strategies, the differences may be decreased if aligning their *PCO* to a common value. The comprehensive impact of these equivalent *PCC* models on positioning needs further investigation.

### *5.1. Virtual Positioning Biases with Equivalent PCC Models*

Following the steps described in Section 3.2, we performed the simulated positioning experiments based on the original $PCC_0$ model of TRM59800.00 NONE in igs14.atx, and a sets of equivalent $PCC_s$ models are obtained according to Equation (18) with $d_{pco}$ = (0, 0, $s$) mm,

$s$ denotes the differences of $PCO$ in the up component between $PCC_0$ and $PCC_s$, and in this experiment, $s$ is from $-10$ to 10 mm with an interval of 1 mm. In addition, the virtual satellites are located in the 1° by 1° grid of the antenna upper hemisphere, and $PCC$ differences from all directions are included in the point positioning. As is described in Section 3.2, position biases in the north, east, and up components along with datum difference $\nabla B$ are estimated and shown in Figure 10. Positioning bias in the up component is all less than 0.01 mm with a different shift $s$ in the $PCO$ up component for L1 and L2 signals; additionally, the biases in the north and east are almost zero within the truncation precision of $10^{-5}$ mm, which is unperceivable or ignored in positioning. It is found that coordinate biases remain quite steady as different $PCC_s$ is applied and even the differences $s$ reach 10 mm. Overall, positioning biases caused by equivalent $PCO/PCV$ sets with centimeter-level differences remain at the 0.01 mm level, which is insignificant for most phase-based applications. The datum difference $\nabla B$ is highly correlated with the intentional shift $s$. In the actual GNSS application, the coefficient of the datum difference $\nabla B$ is the same as the receiver clock or ambiguity, and $\nabla B$ was obviously absorbed into the clock and ambiguity parameter or eliminated by differencing observations between satellites. In addition, the position biases in this virtual point positioning can be used to measure the difference of the two $PCC$ models in the coordinated domain, which is a convenient way of comparing $PCV$ in the whole grid cells.

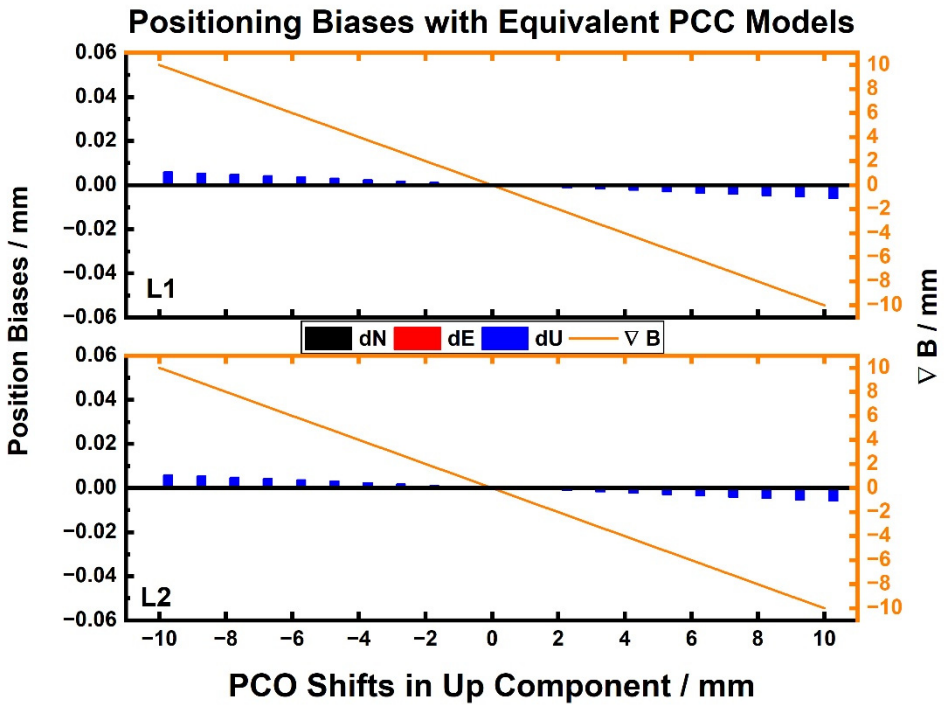


**Figure 10.** Position biases of different $PCC$s models with shifted $PCO$ and $PCV$ combinations.

Based on this experiment, we can conclude that insignificant influences are imposed on the positioning estimate if equivalent $PCC$ models, even with differences at the centimeter level, are applied. Therefore, consistency can be ensured for these $PCC$ models, and it is appropriate to use or replace them without the extra worry of significant $PCC$ biases.

### *5.2. Distribution of Virtual Positioning Biases*

In the actual scenarios, it is impossible for a single receiver to track satellites from all directions, and the $PCC$s are usually sparse and unevenly distributed. Therefore, the impact of $PCC$ on position may vary with the user's location. Researchers have proposed a latitude-dependent model to correct such a position offset [20,21], and it is necessary to investigate the differences in the equivalent $PCC$ models on positioning in such circumstances. We

chose DoY 070 in 2021 as an example and collected the GPS ephemeris and set a virtual station at different locations across global areas, and satellite positions were computed according to the real ephemeris in a timespan from 0:00 to 24:00. Afterward, the virtual ranging observations were calculated if the satellite was above the horizon line, and positioning experiments were performed according to Section 3.2. Here, the station is placed on every grid cell from −180 to 180 degrees in longitude and −85 to 85 degrees in latitude with an interval of 5 degrees. The sampling rate of the satellite position is set to 1 min. In this simulation experiment, we chose the models for L1 of TRM59800.00 NONE in igs14.atx as $PCC_0$.

We first investigated the impact of *PCV* variation on positioning according to Section 3.2. Here, the virtual ranging observation is constructed by $PCC_0(PCO_0/PCV_0)$ and $PCC_1(PCO_1/PCV_1)$. $PCO_1$ is equal to $PCO_0$ and $PCV_1$ is zero. Therefore, only the $PCV_0$ is left in the virtual ranging observations and the position biases reflect the impact of *PCV* on the positioning at different locations. The distributions of the positioning biases in the north, east, and up components along with the position dilution of precision (PDOP) are shown in Figure 11. The positioning biases induced only by *PCV* are not evenly distributed, and the biases in the north and up components are significantly correlated with the latitude. A weaker correlation can be found between bias in the east component with the longitude. The 95th percentile of the PDOP was calculated over one week, and the distribution of the PDOP is also latitude dependent but not the same as the position biases, which means that the variation in the *PCC* contributes to the positioning biases. For the magnitude, bias from 16~28 mm in the up component contributes to most of the positioning error budget, which is reasonable for a large variation range of *PCV* with zenith and a small range with azimuth. Furthermore, biases, especially in the up component, will increase to the decimeter level if $PCO_1$ is set to zero. However, the biases induced by the *PCO* at different locations are the same since the *PCO* can be viewed as constant shifts in the local north-east-up coordinates. It should be noted that the positioning bias distributions are not fixed in Figure 11 and will change if different *PCC* models or constellations are applied in this simulated experiment. In a word, the influence of *PCC* on positioning cannot be ignored in high-precision applications, and should be corrected with accurate *PCC* models.

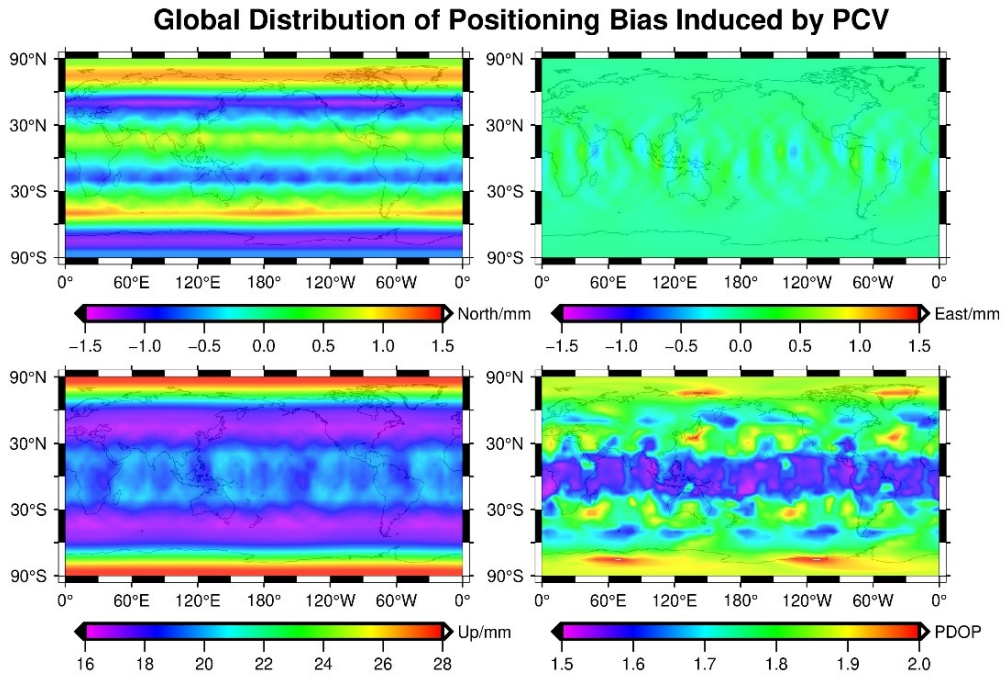


**Figure 11.** Global distribution of positioning biases induced from *PCV* for TRM59800 in L1.

Next, we construct an equivalent $PCC_2(PCO_2/PCV_2)$ model with $d_{pco}$ = (0, 0, −10) mm between $PCO_0$ and $PCO_2$, and $PCV_2$ is obtained by transformation of $PCV_0$ according to Equation (18). Moreover, the simulated point positioning is performed using $PCC_0$ and $PCC_2$. Finally, the distributions of the positioning biases between $PCC_0$ and $PCC_2$ are shown in Figure 12.

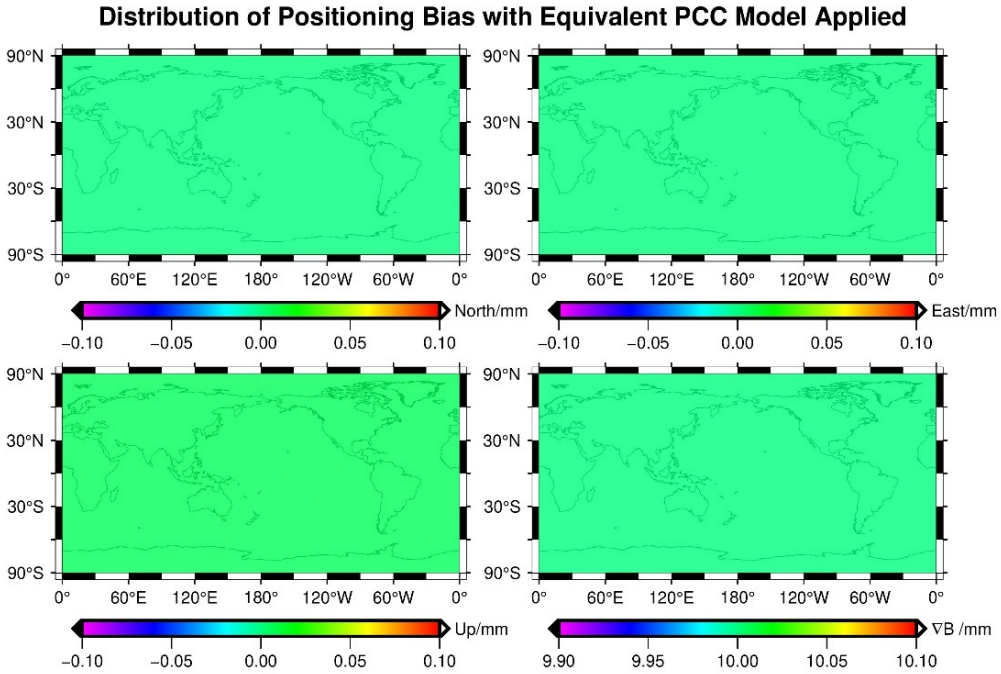


**Figure 12.** Distribution of simulated positioning biases between equivalent *PCC* models for antenna TRM59800.00, L1.

It can be clearly seen that positioning biases are dramatically decreased to the 0.01 mm level, which is acceptable for normal GNSS applications. Additionally, the significantly uneven distribution of positioning biases disappears, which shows a high consistency between the equivalent $PCC_2$ model and original $PCC_0$ model at different location. In particular, the distribution of the datum difference $\nabla B$ between the two *PCC* models is negatively correlated with biases in the upper component, and the −10 mm difference is perfectly absorbed into $\nabla B$ rather than the coordinates, which is the same as the clock parameter in field data positioning. This example can validate the self-consistency of the equivalent *PCC* models. Therefore, it can be safely concluded that almost no positioning biases are induced if an equivalent *PCC* model is applied, even if large numerical differences might exist between them. The same positioning investigations with the equivalent *PCC* model were performed on the other *PCC* models available in igs14.atx, and the results of the simulated point positioning biases show high consistency.

### *5.3. Positioning Validation*

For antenna JAV_RINGANT_G3T NONE, simulation positioning experiments of the *PCC* models from robot calibration in igs14.atx and anechoic chamber calibration from igsR3.atx are performed, and the biases in L1 and L2 are listed in Table 2. The biases in the simulated positioning are all within 1 mm in the north, east, and up component, which is obviously smaller than the direct numerical differences in the *PCC* models.

**Table 2.** Biases in the *PCC* model for JAV_RINGANT_G3T NONE between robot calibration and anechoic chamber calibration in simulated positioning (unit:mm).

| Bias | N | E | U |
|---|---|---|---|
| L1 | −0.16 | 0.09 | −0.55 |
| L2 | 0.51 | −0.35 | 0.13 |

Apart from the simulated positioning experiments, static PPP and baseline solution are performed to validate the simulated positioning experiment and consistency of the *PCC* model for antenna JAV_RINGANT_G3T NONE. In this case, static field GNSS data from two IGS station BIK0 and POL2 are collected from DoY 071 to 077 in 2021, and station BIK0 is equipped with antenna JAV_RINGANT_G3T NONE whose *PCC* model was analyzed in the previous discussion. For this special antenna, the *PCC* model from robot calibration is chosen from igs14.atx with anechoic chamber calibration from igsR3.atx. In the data processing, the two *PCC* models will be applied, respectively, and the differences in the coordinate series will be analyzed to investigate the consistency of the two *PCC* models.

At first, the typical PPP solution is performed for station BIK0 using ionosphere-free (IF) combination of L1/L2, and the *PCC* model from robot and anechoic chamber calibration are applied, respectively. The root mean square (RMS) of the differences in the coordinate series are listed in Table 3. The average RMS of the PPP solution differences are 1.28, 3.49, and 3.73 mm in the horizon, up, and 3D component. It can be easily seen that the RMS is smaller than the direct numerical differences in the original *PCO*/*PCV* sets listed in Table 1, where differences for a single frequency can reach −6.02 mm in L1 and −3.86 mm in L2. However, the difference in the PPP solution is larger than the simulated point positioning biases listed in Table 3. This might be caused by the IF observation, and the difference for the IF observation should be amplified by the differences in L1 and L2 combined.

**Table 3.** RMS of baseline and PPP solution differences between the *PCC* model from robot and chamber calibration (unit:mm).

| DoY | PPP Solution | | | Baseline Solution | | | | | |
|---|---|---|---|---|---|---|---|---|---|
| | IF | | | L1 | | | L2 | | |
| | Horizon | Up | 3D | Horizon | Up | 3D | Horizon | Up | 3D |
| 071 | 1.27 | 3.51 | 3.74 | 0.15 | 0.13 | 0.21 | 0.60 | 0.63 | 0.88 |
| 072 | 1.28 | 3.53 | 3.77 | 0.11 | 0.10 | 0.17 | 0.58 | 0.34 | 0.71 |
| 073 | 1.28 | 3.50 | 3.74 | 0.12 | 0.14 | 0.20 | 0.61 | 0.41 | 0.74 |
| 074 | 1.28 | 3.51 | 3.75 | 0.30 | 0.35 | 0.48 | 0.95 | 0.51 | 1.15 |
| 075 | 1.28 | 3.49 | 3.73 | 0.16 | 0.15 | 0.23 | 0.63 | 0.32 | 0.72 |
| 076 | 1.28 | 3.52 | 3.75 | 0.13 | 0.06 | 0.16 | 0.56 | 0.47 | 0.74 |
| 077 | 1.29 | 3.37 | 3.61 | 0.13 | 0.13 | 0.20 | 0.59 | 0.40 | 0.72 |
| mean | 1.28 | 3.49 | 3.73 | 0.16 | 0.15 | 0.24 | 0.65 | 0.44 | 0.81 |

Furthermore, the single frequency baseline solution of BIK0−POL2 is performed to investigate the consistency of the two *PCC* models. The baseline positioning was conducted through a forward Kalman filter with double-differencing observation. The coordinate differences series of the baseline positioning by applying different *PCC* models at DoY 071, 2021 are shown in Figure 13. For L1, the differences in the coordinates between the two *PCC* models are quite small and stable. The magnitudes of the positioning differences in the north, east, and up components are all less than 1 mm. However, the numerical *PCO* differences in the two models between robot and chamber calibration can exceed 6 mm, as presented in Table 1. The *PCV* differences can reach 3 or 4 mm in certain directions, as shown in Figure 9. Although larger differences and variations can be found for L2

compared with L1, the magnitudes remain within 1 mm. This phenomenon is consistent with the result shown in Figure 9. After *PCO* is aligned with the same values, the *PCV* differences are still larger with L2 than with L1. In other words, the numerical differences in the *PCC* model up to 6 mm are seldomly embodied in the positioning estimation. The effect of the *PCO* differences might be canceled out by the *PCV* differences if equivalent *PCC* models are applied.

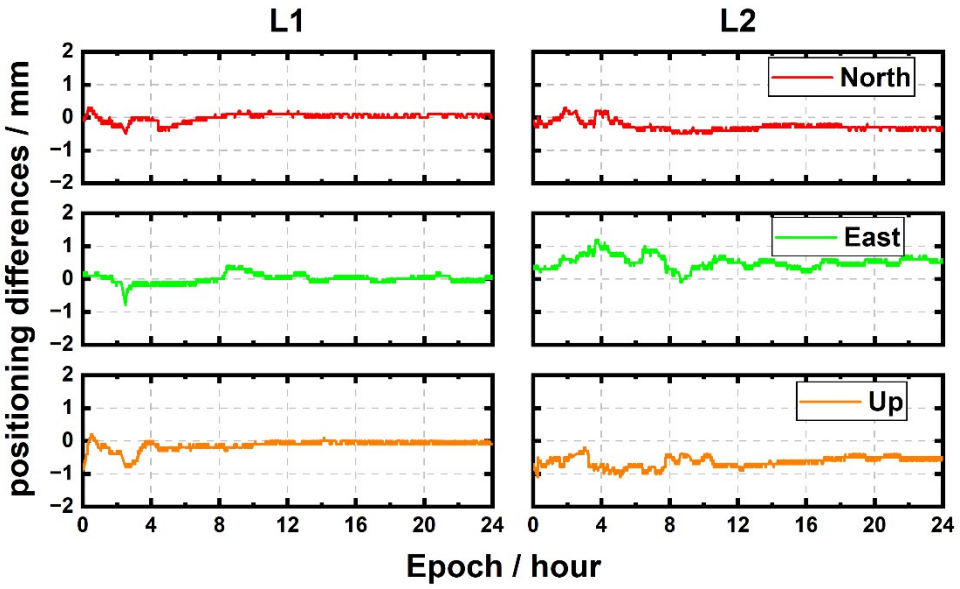


**Figure 13.** Differences in the north, east, and up component of baseline positioning between IGS Station POL2 and BIK0 with the *PCC* model from robot and chamber calibration.

To further investigate and validate the previous conclusion, the baseline solution of BIK0−POL2 was performed for 7 days, and the RMS of the coordinate differences in the horizon, up, and 3D components using the *PCC* model from robot and chamber calibration are calculated and listed in Table 3. For L1, the differences induced by the *PCC* model are all less than 0.5 mm, while the counterparts for L2 are slightly larger, ranging from 0.72 to 1.15 mm. In terms of the average RMS over 7 days, differences of 0.16, 0.15, and 0.52 mm in the horizon, up, and 3D component in L1 were observed and 0.65, 0.44, and 0.81 mm for L2. The comparison of the baseline solution with the two *PCC* models with large numerical differences in *PCO* and *PCV* showed a comparably smaller impact on coordinate estimation. In addition, the coordinate difference in the baseline solution is more consistent with the simulated point positioning result in Table 2 than that in the PPP solution, which indicates the advantages of the baseline solution over the PPP solution in *PCC* validation.

Based on the simulation analysis and field data positioning, we can conclude that for a certain antenna, its *PCC* model could be presented in several sets of *PCO*s and *PCV*s. Even if large numerical differences may exist, these different *PCC* models can still be viewed as equivalent or approximately equivalent.

## 6. Conclusions

In this contribution, we analyzed the factors that may be responsible for large numerical differences in existing *PCC* models and investigated the mutual impact of *PCO* and *PCV* in calibration and positioning through simulation and field experiments. The main conclusions based on these experiments are as follows.

Numerical differences at the sub-centimeter level in *PCO* or *PCV* exist for some *PCC* models by comparing them between different versions of ANTEX files. However, the magnitude of these differences is apparently larger than the calibration precision of 1.0 or even 0.5 mm.

The simulation and field experiments showed that the *PCO* and *PCV* are highly coupled with each other in calibration. First, omitting *PCV* in *PCO* estimation disturbs the *PCO* estimates, and the disturbance in *PCO* forwardly affects the *PCV* extraction. Thus, different strategies in calibration might lead to different *PCO*/*PCV* sets, and it explains the *PCC* differences from different institutions. In the virtual estimation of *PCO*, the elevation mask was chosen to decide what range of *PCV* will be included in the *PCO* estimation, and the result shows that the up component of the *PCO* estimates will vary beyond 10 mm if the elevation mask is set from 0 to 30 degrees. In the simulated estimation of *PCV*, several intentional shifts were added to the original *PCO* value. The estimated *PCV* values show synchronized variation with the shifts in *PCO* and will perfectly compensate for the shifts. Therefore, a specific *PCC* model can be expressed in multiple *PCO*/*PCV* sets in calibration if different strategies are applied, and these *PCC* models are indeed equivalent.

Then, we investigated the impact of *PCC* on positioning and the applicability of an equivalent *PCC* model. Considering the actual constellation, positioning biases induced in *PCV* are related to latitude or longitude. The variation in position biases is correlated with the magnitude of the *PCV*. However, these positioning biases decrease to the 0.01 mm level if an equivalent *PCC* model is applied. The results of the positioning experiments can prove that these different *PCC* models with large numerical differences in *PCO*/*PCV* for one antenna are equivalent in positioning.

In this contribution, an extra constant datum parameter *B* in the *PCC* model in addition to the classical *PCO*/*PCV* set was applied. With the help of parameter B, one set of *PCC* can be transformed to another equivalent set with certain numerical differences in *PCO* and *PCV* while their consistency in positioning remains after the *PCC* transformation. An extreme case of antenna JAV_RINGANT_G3T NONE was investigated in detail. For this antenna, its *PCC* models by robot and anechoic chamber calibration are presented in igs14.atx and igsR3.atx, respectively, while their numerical differences can reach 6 mm. However, the differences dramatically decrease to the 1 mm level after following the alignment procedures, which means that the two *PCC* models are approximately equivalent. Comparing the two *PCC* models using the simulated point positioning described in this contribution, the differences in the coordinate domain are $(-0.16, 0.09, -0.55)$ mm for L1 and $(0.51, -0.35, 0.13)$ mm for L2 in the north, east, and up component, which is apparently smaller. In a positioning experiment with field GNSS observation, the coordinate differences induced just by the two *PCC* models are also less than 1 mm in the. baseline solution and 4 mm in the PPP solution. The better consistency in the baseline solutions might be explained by the single frequency observation, since the ionosphere-free combination is used in the PPP solution. The comparison of simulation and field positioning can validate the correctness of the constant datum parameter *B* and the alignment procedures.

Based on the work in this contribution, we hope to provide a new vision to understand the *PCC* model and provide a comprehensive method to evaluate its impact on calibration and positioning.

**Author Contributions:** Conceptualization, Z.H. and R.Z.; methodology, Z.H. and R.Z.; validation, X.L. and C.L.; data curation, H.K.; writing—original draft preparation, R.Z.; writing—review and editing, G.W., H.C. and L.C.; supervision, Q.Z.; funding acquisition, Z.H. and Q.Z. All authors have read and agreed to the published version of the manuscript.

**Funding:** This work was sponsored by the funds of the National Natural Science Foundation of China (Grant No. 42030109, 41774007), Young Elite Scientists Sponsorship Program by CAST (YESS20200308), China Postdoctoral Science Foundation (2021M690192) and Beijing Postdoctoral Research Foundation (2021-ZZ-088) and Beijing Nova Program (2021060).

**Institutional Review Board Statement:** Not applicable.

**Informed Consent Statement:** Not applicable.

**Data Availability Statement:** The ATX file of igs05.atx, igs08.atx, igs14.atx in this work can be found from https://files.igs.org/pub/station/general/ (accessed on 18 January 2022) and igsR3.atx can be found from http://ftp.aiub.unibe.ch/users/villiger/ (accessed on 18 January 2022). The observations and ephemeris can be found at ftp://igs.gnsswhu.cn/pub/gps/data/daily/2022/ (accessed on 18 January 2022).

**Acknowledgments:** The authors would like to thank IGS for providing antenna phase center models and high quality GNSS data.

**Conflicts of Interest:** The authors declare no conflict of interest.

## References

1. Tranquilla, J.M.; Colpitts, B.G. GPS Antenna Design Characteristics for High-Precision Applications. *J. Surv. Eng.* **1989**, *115*, 2–14. [CrossRef]
2. Rocken, C.; Meertens, C.; Stephens, B.; Braun, J.; VanHove, T.; Perry, S.; Ruud, O.; McCallum, M.; Richardson, J. UNAVCO Academic Research Infrastructure (ARI) Receiver and Antenna Test Report. UNAVCO Boulder Facility International Report. Available online: https://www.unavco.org/projects/project-support/development-testing/publications/ari_test.pdf (accessed on 18 January 2022).
3. Schupler, B.R.; Clark, T.A.; Allshouse, R.L. Characterizations of GPS user antennas: Reanalysis and new results. In *GPS Trends in Precise Terrestrial, Airborne, and Spaceborne Applications*; Springer: Berlin/Heidelberg, Germany, 1996; pp. 328–332.
4. Mader, G.L. GPS Antenna Calibration at the National Geodetic Survey. *GPS Solut.* **1999**, *3*, 50–58. [CrossRef]
5. Wübbena, G.; Schmitz, M.; Menge, F.; Seeber, G.; VÖLKSEN, C. A new approach for field calibration of absolute GPS antenna phase center variations. *Navigation* **1997**, *44*, 247–255. [CrossRef]
6. Menge, F.; Seeber, G.; Volksen, C.; Wübbena, G.; Schmitz, M. Results of absolute field calibration of GPS antenna *PCV*. In Proceedings of the 11th International Technical Meeting of the Satellite Division of The Institute of Navigation (ION GPS 1998), Nashville, TN, USA, 15–18 September 1998.
7. Bergstrand, S.; Jarlemark, P.; Herbertsson, M. Quantifying errors in GNSS antenna calibrations. *J. Geod.* **2020**, *94*, 105. [CrossRef]
8. Krzan, G.; Dawidowicz, K.; Wielgosz, P. Antenna phase center correction differences from robot and chamber calibrations: The case study LEIAR25. *GPS Solut.* **2020**, *24*, 747. [CrossRef]
9. Darugna, F.; Wübbena, J.B.; Wübbena, G.; Schmitz, M.; Schön, S.; Warneke, A. Impact of robot antenna calibration on dual-frequency smartphone-based high-accuracy positioning: A case study using the Huawei Mate20X. *GPS Solut.* **2021**, *25*, 2621. [CrossRef]
10. Villiger, A.; Dach, R.; Schaer, S.; Prange, L.; Zimmermann, F.; Kuhlmann, H.; Wübbena, G.; Schmitz, M.; Beutler, G.; Jäggi, A. GNSS scale determination using calibrated receiver and Galileo satellite antenna patterns. *J. Geod.* **2020**, *94*, 6109. [CrossRef]
11. Geiger, A. Modeling of phase center variation and its influence on GPS-positioning. In *GPS-Techniques Applied to Geodesy and Surveying*; Groten, E., Strauß, R., Eds.; Springer: Berlin Heidelberg, Germany, 1988; pp. 210–222, ISBN 978-3-540-45962-0.
12. Wübbena, G.; Schmitz, M.; Menge, F.; Böder, V.; Seeber, G. Automated absolute field calibration of GPS antennas in real-time. In Proceedings of the International Technical Meeting, ION GPS-00, Salt Lake City, UT, USA, 19–23 September 2000.
13. Bilich, A.; Mader, G.L. GNSS absolute antenna calibration at the national geodetic survey. In Proceedings of the 23rd International Technical Meeting of The Satellite Division on the Institute of Navigation, Portland, OR, USA, 1–24 September 2010; pp. 1369–1377.
14. Kröger, J.; Kersten, T.; Breva, Y.; Schön, S. Multi-frequency multi-GNSS receiver antenna calibration at IfE: Concept-calibration results-validation. *Adv. Space Res.* **2021**, *68*, 4932–4947. [CrossRef]
15. Riddell, A.; Moore, M.; Hu, G. Geoscience Australia's GNSS antenna calibration facility: Initial results. In Proceedings of the IGNSS Symposium 2015 (IGNSS2015), Gold Coast, Australia, 14–16 July 2015.
16. Rothacher, M.; Schmid, R. ANTEX: The Antenna Exchange Format, Version 1.4; 15 September 2010. Available online: https://files.igs.org/pub/station/general/antex14.txt (accessed on 18 January 2022).
17. Willi, D.; Koch, D.; Meindl, M.; Rothacher, M. Absolute GNSS Antenna Phase Center Calibration with a Robot. In Proceedings of the 31st International Technical Meeting of The Satellite Division of the Institute of Navigation (ION GNSS+ 2018), Miami, FL, USA, 24–28 September 2018; pp. 3909–3926.
18. Hu, Z.; Zhao, Q.; Chen, G.; Wang, G.; Dai, Z.; Li, T. First Results of Field Absolute Calibration of the GPS Receiver Antenna at Wuhan University. *Sensors* **2015**, *15*, 28717–28731. [CrossRef] [PubMed]
19. Schön, S.; Kersten, T. Comparing Antenna Phase Center Corrections: Challenges, Concepts and Perspectives. In Proceedings of the IGS Analysis Workshop, Pasadena, CA, USA, 23–27 June 2014.
20. Baire, Q.; Bruyninx, C.; Legrand, J.; Pottiaux, E.; Aerts, W.; Defraigne, P.; Bergeot, N.; Chevalier, J.M. Influence of different GPS receiver antenna calibration models on geodetic positioning. *GPS Solut.* **2014**, *18*, 529–539. [CrossRef]
21. Rebischung, P.; Griffiths, J.; Ray, J.; Schmid, R.; Collilieux, X.; Garayt, B. IGS08: The IGS realization of ITRF2008. *GPS Solut.* **2012**, *16*, 483–494. [CrossRef]